Resolving Phase: Inversion of SWI-Phase Data in Order to Obtain its Sources Utilizing the Concept of a Generalized Lorentzian Approximation

F. Schweser[1], M. Hütten[1], B. W. Lehr[1], A. Deistung[1], D. Güllmar[1], and J. R. Reichenbach[1]
[1]Medical Physics Group, Department of Diagnostic and Interventional Radiology, Jena University Hospital, Jena, Germany

INTRODUCTION – Susceptibility weighted MR phase data provide anatomical contrast complementary to magnitude data [1-3] by directly reflecting local magnetic field changes. However, the origin of phase contrast is not yet fully understood. Sources of the phase contrast are currently attributed to magnetic susceptibility distribution [4], chemical exchange with proteins [5], electronic screening effects [6], and the magnetic architecture at the (sub-)cellular level [7]. We decoupled these components by inverting volunteer phase data of the brain that was acquired at different orientations of the head with respect to the magnetic field in order to obtain the sources and their contributions.

THEORY – The magnetic field distortion $b_\chi(\vec{r})$ due to magnetic susceptibility contributions $\chi(\vec{r})$ is non-local and depends on the orientation of $\chi(\vec{r})$ with respect to the main magnetic field $\vec{B}_0$: $b_\chi = b_\chi(\vec{r}, \vec{B}_0)$ [4]. Local shifts due to (high) anisotropy at (sub-)cellular level (e.g., due to neuronal fibers) may be described by the generalized Lorenzian approximation [7]: $b_a = b_a(\vec{r}, \theta, \chi_a) = -1/2\chi_a(\cos^2\theta - 1/3)$, where theta is the angle between anisotropy direction and the main magnetic field. Taking into account contributions from rotation-invariant local effects $b_\sigma(\vec{r})$, e.g., electronic screening or chemical exchange effects, yields for the total magnetic field shift: $b(\vec{r}, \vec{B}_0, \theta) = b_\chi + b_\sigma + b_a$. Since the dependence of these three contributions on the direction of $\vec{B}_0$ is different data-acquisition at different orientations of the object to $\vec{B}_0$ should enable decoupling of the underlying sources of phase contrast.

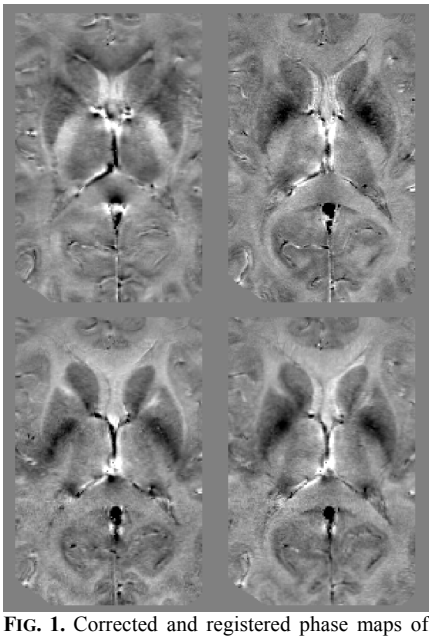

FIG. 1. Corrected and registered phase maps of the different orientations of the head showing basal ganglia (-0.8…0.8 rad).

MATERIALS AND METHODS

Data Acquisition: High-resolution volunteer data of the whole brain were acquired with the TOF-SWI sequence [8] (TE1/TE2/TR/FA/BW1/BW2 = 3.38ms/22ms/30ms/20°/271Hz/px/93Hz/px, voxel size 0.6×0.6×0.6 mm³, 75% PF in phase and slice encoding direction) and a DTI-sequence (TE/TR/b-value/nDirections = 91ms/6900ms/1000 s·mm^{-2}/76, voxel size 2.5×2.5×2.5 mm³) on a 3T MR-scanner (Tim Trio, Siemens Medical Solutions) using a 12-channel head-matrix coil. Four acquisitions were performed with the head tilted approx. -35°, -17°, 4°, and 50° about the x-axis (left-right-axis) with respect to the magnetic field orientation.

Pre-Processing: Multi-channel phase images were combined using uniform sensitivity reconstruction [9] and 3D phase unwrapping [10] was applied to resolve phase aliasing. Background field contributions were removed based on the harmonic-function mean-value property [11]. Voxels with unreliable phase values (unwrapping artifacts and low SNR) were masked and excluded from further processing. The ToF-SWI and DTI data sets were registered using FLIRT [12] to the 4°-acquisition. DTI-tensor maps were reconstructed and the angles θ between the largest Eigenvector and $\vec{B}_0$ were calculated.

Inversion: Inversion of phase information was facilitated by a spatial-domain algorithm [13]. The algorithm was extended to handle multiple phase datasets simultaneously and to solve the equation system $b = A\chi + \sigma + B\chi_a$ with respect to χ, χ_a, and σ. In order to consider only anisotropy information of large fiber bundles χ_a was restricted to voxels with a fractional anisotropy above 0.6.

RESULTS – The registered phase images of the four orientations in Fig. 1 reflect the orientation dependency of the magnetic field which is nicely discernable for venous vessels and the globus pallidus. Inversion using the four registered phase maps reveals volumes of the magnetic susceptibility, local rotational-invariant shift, and (sub-cellular) anisotropy induced susceptibility. Representative slices of these volumes are presented in Fig. 2 and 3. Note that the extra-vascular field inhomogeneity was successfully compensated in all susceptibility maps (arrows). The contrast between gray and white matter is preserved in the susceptibility map and nearly diminishes in the rotation-invariant data (Fig. 3, box).

DISCUSSION AND CONCLUSIONS – We have demonstrated a novel method to compute magnetic-susceptibility maps and maps of rotation-invariant and rotation-variant frequency-shifts *in vivo* by taking into account anisotropy of large fiber-bundles. In contrast to previously published approaches [5] quantification was facilitated without voxel-based constraints. Thus, the approach enables *in vivo* exploration of the nature of phase contrast. We have shown that gray-to-white matter contrast in phase images is dominated by sources from magnetic susceptibilities rather than macro-molecular exchange processes. This finding is in excellent agreement with *in vitro* studies which indicated that iron (and to a lesser extent myelin) contribute significantly to phase contrast [13].

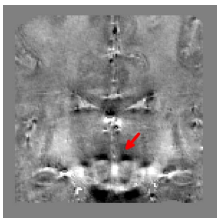

FIG. 4. Phase map corresponding to Fig. 2-bottom (-0.8…0.8 rad).

REFERENCES – [1] Rauscher A et al. *Am J Neuroradiol,* 26(4):736-42, 2005. [2] Deistung A et al. *Magn Reson Med*, 60(5):1155-68, 2008. [3] Duyn JH et al. *Proc Natl Acad Sci Unit States Am,* 104(28):11796-801, 2007. [4] Marques JP and Bowtell R. *Concepts Magn Reson B Magn Reson Eng*, 25(1):65-78, 2005. [5] Luo J et al. *J Magn Reson* (in press) [6] de Rochefort L et al. *Magn Reson Med,* 60(4):1003-9, 2008. [7] He X and Yablonskiy DA. *Natl Acad Sci U S A,* 106(32):13558-63, 2009. [8] Deistung A et al. *J Magn Reson Imag*, 29(6):1478-84, 2009. [9] Ros C et al. *ISMRM*, p1265, 2008. [10] Abdul-Rahman HS et al. *Appl Optics*, 46(26):6623-35, 2007. [11] Schweser F et al. *ISMRM,* 2010 (submitted). [12] Jenkinson M et al. *NeuroImage*, 17(2):825-841, 2002. [13] Deistung A et al. *ISMRM*, p2931, 2009.

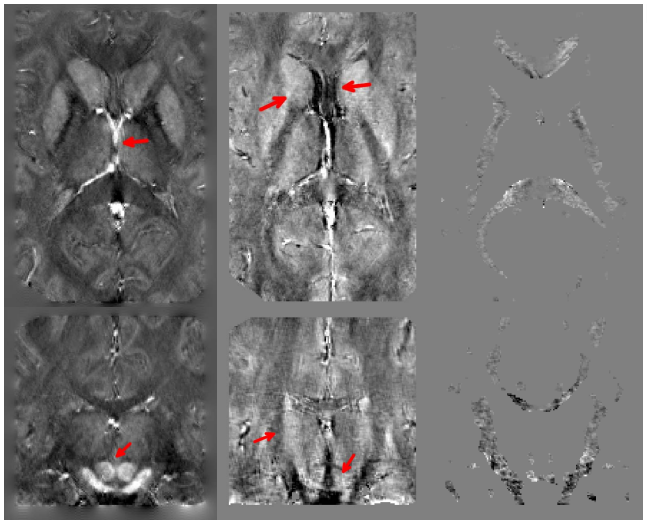

FIG. 2. Exemplary slices of the susceptibility map (left, -0.1…0.2 ppm), rotation-invariant frequency shift-map (middle, -0.02…0.02 ppm), and anisotropy-susceptibility map (right, -0.05…0.05 ppm). Phase maps corresponding to (top) are shown in Fig. 1.

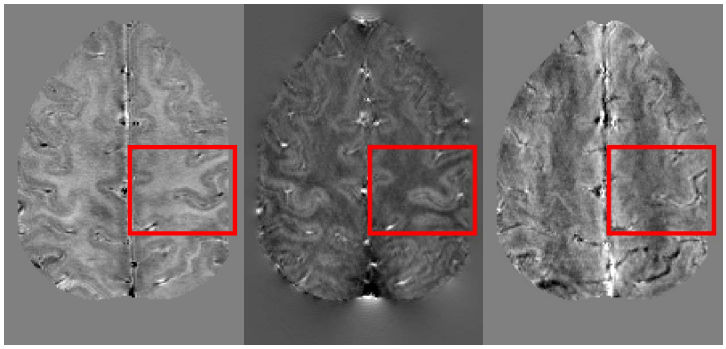

FIG. 3. White and gray-matter contrast in phase map (left, -0.8…0.8 rad), susceptibility map (middle, -0.1…0.2 ppm), and rotation-invariant shift map (right, -0.02…0.02 ppm).